ADVANCES IN GEODESY AND GEOINFORMATION
(formerly GEODESY AND CARTOGRAPHY)
Vol. 72, no. 2, article no. e45, 2023

https://doi.org/10.24425/agg.2023.146157

Original paper

Environmental mapping of Burkina Faso using TerraClimate data and satellite images by GMT and R scripts

Polina Lemenkova[1]*, Olivier Debeir[2]

[1]Universität Salzburg, Salzburg, Austria
e-mail: polina.lemenkova@plus.ac.at; ORCID: http://orcid.org/0000-0002-5759-1089
[2]Université Libre de Bruxelles, Brussels, Belgium
e-mail: olivier.debeir@ulb.be; ORCID: http://orcid.org/0000-0002-6461-1551

*Corresponding author: Polina Lemenkova, e-mail: polina.lemenkova@plus.ac.at

Received: 2023-02-25 / Accepted: 2023-06-07

Abstract: In this paper, the climate and environmental datasets were processed by the scripts of Generic Mapping Tools (GMT) and R to evaluate changes in climate parameters, vegetation patters and land cover types in Burkina Faso. Located in the southern Sahel zone, Burkina Faso experiences one of the most extreme climatic hazards in sub-saharan Africa varying from the extreme floods in Volta River Basin, to desertification and recurrent droughts.. The data include the TerraClimate dataset and satellite images Landsat 8-9 Operational Land Imager (OLI) and Thermal Infrared (TIRS) C2 L1. The dynamics of target climate characteristics of Burkina Faso was visualised for 2013-2022 using remote sensing data. To evaluate the environmental dynamics the TerraClimate data were used for visualizing key climate parameter: extreme temperatures, precipitation, soil moisture, downward surface shortwave radiation, vapour pressure deficit and anomaly. The Palmer Drought Severity Index (PDSI) was modelled over the study area to estimate soil water balance related to the soil moisture conditions as a prerequisites for vegetation growth. The land cover types were mapped using the k-means clustering by R. Two vegetation indices were computed to evaluate the changes in vegetation patterns over recent decade. These included the Normalized Difference Vegetation Index (NDVI) and the Soil-Adjusted Vegetation Index (SAVI) The scripts used for cartographic workflow are presented and discussed. This study contributes to the environmental mapping of Burkina Faso with aim to highlight the links between the climate processes and vegetation dynamics in West Africa.

Keywords: environmental monitoring, cartography, image processing, sub-saharan Africa, R programming

1. Introduction

Despite years of active research, the role of climate in vegetation remains an unsolved problem for a number of reasons. First, the response of vegetation to climate has a non-linear character and complex nature with both direct and indirect effects. A variety of physical geographic and climatic factors directly contribute to the development of the vegetation and control the growth and health of vegetation. These include, for instance, such parameters as temperature and solar radiation, moisture and precipitation, wind and relief morphometry. The indirect processes include the effects from the climatic parameters on soil conditions, health of microorganisms and fauna that constitute a vital part of the complex biochemical cycle and food chain.

Second, revealing complex interactions between vegetation and climate requires the analyses of large datasets to highlight the links and correlations between the variables. This necessarily requires the use of the advanced methods of big data processing. Even moderate changes in climate variables often result in a noticeable change in vegetation patters in a spatio-temporal perspective. These can be analysed using technical methods of predictive modelling and simulation of the spatial distribution of the vegetation patterns across a landscape based on climatic and environmental variables as input data. All of these factors significantly alter our understanding of how climate-vegetation links function.

Third, the machine-based quantification of complex climate-vegetation system requires considering not only a full range of the climatic and environmental parameters that affect vegetation condition and growth but also a temporal delay in reaction of plant species on climate change. Thus, a complete change in land cover types and landscape patterns, including boundaries of habitats, may take up to several seasons. Further, simulating climate-environmental relationships also needs to handle other external factors such as urban growth and industrial heat sources, water pollution and soil contaminations, as well as changes in local topography which may have a human-induced (construction works, career and mining) and natural origin (landslides, soil subsidence).

While all of these factors have been studied (Mather, 1987; Bocksberger et al., 2016), the problem of the developing advanced methods of data processing is the only one that we believe is still largely unsolved. Most commercially deployed Geographic Information System (GIS) are based on the predefined functionality of the software and have limited embedded algorithms of data processing. They sometimes employ simple methods of image manipulation which do not take into consideration real features of datasets. Processing large geospatial datasets becomes even more critical for standard GIS tools that rely on manual data processing. In contrast, advance solutions proposed through scripts and programming tools enable to handle geospatial data automatically and accurately, which is the main focus on this paper.

Satellite image processing are very popular methods successfully used in many applications of climate and environmental studies including such topics as land cover / land use changes (Machwitz et al., 2008; Ouedraogo et al., 2010; Zoungrana et al., 2015), computation of the vegetation indices, assessment of deforestation and estimation of burned areas (Musyimi et al., 2017), mapping plant species distribution (Devineau et

al., 2010) to mention a few. The fundamental importance of remotely sensed data in Earth observation and environmental monitoring is discussed in a variety of papers (Wilmet, 2010). The main idea behind these methods is to classify remote sensing data by finding spatial patterns in the types of vegetation coverage contrasting from other land cover types (e.g., water areas, urban zones, roads). The identification of vegetation area and land cover types is based on the analysis of the spectral signatures of the pixels on the image which differ in spectral properties of that object in various bands of the satellite image (Richards, 2013). Such fundamental properties of various objects on the Earth's surface enables their discrimination on the satellite images.

The dynamics in changes of land cover types can be analysed using the correspondent series of images showing the same spatial extent for various years as time series. However, these approaches are mostly done using the traditional software developed for satellite image processing, such as Erdas Imagine or ArcGIS, which are incomplete in two major aspects: (i) Although handling the datasets using scripts is possible using widgets, e.g., developed with the ERDAS Macro Language (EML) or ArcPy in ArcGIS, both the software remain mostly GUI-oriented. Therefore, manual operational routine in image processing remains high; (ii) it is not possible to operate with data using console which significantly optimizes the machine workflow, compared to the traditional state-of-the-art software. Handling data by scripts run from the console optimizes the workflow though machine-based automation of data processing which becomes faster and more efficient.

Algorithms for integrating advanced methods into satellite image analysis and cartographic data processing have been proposed earlier. Vanhuysse et al. (2017) reported a case of mapping urban land cover from the Very High Resolution (VHR) optical imagery using the Object-Based Image Analysis (OBIA) approach and WorldView-3 stereo imagery. Van Teeffelen et al. (2001) used the IKONOS image as a source of high spatial resolution remote sensing data for spectral-based image classification applying contextual image processing techniques with size of pixel adjusted to the urban buildings. Wagner and Scipal (2000) formulated the approach of the large-scale soil moisture mapping using ERS scatterometer data to derive the parameters of climatic conditions that are well reflected in the remotely sensed data.

The scenes of Moderate Resolution Imaging Spectrometer (MODIS) were integrated from 2000 to 2012 as time series for water monitoring using a latitudinal threshold gradient approach in a semi-arid region of West-Africa (Moser et al., 2014; Zoungrana et al., 2018). They evaluated yearly cumulative spatiotemporal changes in water extents and assessed their correlation with the occasion of the drought seasons. Miura et al. (2019) used a similar strategy to generate a series of Sentinel-1A images and analyse the repeat cycle of scenes covering the Sapone region in Burkina Faso. Kanmegne Tamga et al. (2023) also used space borne optical Sentinel-1A data integrated with the Synthetic Aperture Radar (SAR) and Light Detection and Ranging (LiDAR) data for deriving the information on the aboveground biomass which is an important indicator of the carbon cycle serving as one of the parameters of climate change in monitoring global terrestrial ecosystem. High resolution SAR images were applied to perform the hydrologic RS-based modelling in the Sahel region of Burkina Faso (Martino et al., 2011).

We argue, however, that nearly all the existing research papers on environmental mapping of Burkina Faso have focused on using the traditional GIS (Augusseau et al., 2001; Cecchi et al., 2008; Dimobe et al., 2015; Kadeba et al., 2015; Forkuor et al., 2018; Idrissou et al., 2022). Such approaches reflected the convenient functionality and characteristics of the most popular GIS software with Graphical User's Interface (GUI) such as Erdas Imaging, ArcGIS, ENVI GIS, Idrisi GIS, SAGA GIS and others. In contrast, the open-source geospatial toolsets and approaches offer more advanced performance of cartographic data processing in terms of computational effectiveness, speed and effectiveness of mapping. Moreover, a high level of automation and repeatability of scripts enables optimization of the image classification workflow which results in a higher accuracy. Finally, for developing countries, the cost of ESRI products, ENVI GIS or other commercial geospatial software can be a serious factor, while GMT and R are free toolsets available openly to everyone.

In this work, we consider the problem of climate and environmental mapping of Burkina Faso using programming methods. Over the last few years, this topic has received a growing amount of attention in the Earth sciences and geospatial community (Landmann et al., 2008; Dimobe et al., 2022a, Lemenkova and Debeir, 2023). We considered the existing applications of scripting languages in Earth science to propose an effective and efficient scripting algorithms by Generic Mapping Tools (GMT) (Wessel and Smith, 1991) and R (R Core Team, 2022) for cartographic data processing and image analysis. We used scripts of GMT and R that automate the workflow of the geospatial data processing, image classification and map generation, thereby facilitating the environmental analysis based on the remote sensing data processing. The proposed algorithms of GMT and R perform favorably against the state-of-the-art GIS software on image processing in terms of accuracy and robustness.

The GMT and R applied for cartographic tasks demonstrate a high level of usability and a faster workflow through automation and a console-based approach. In particular, such methods are useful for a pairwise comparison of several environmental parameters when a series of maps should be plotted for different target years. In such cases, scripts were optimized to highlight the variability of the continuum fields of the represented climatic variables using the adjusted colour map palettes. Such strategy produces a good recognition accuracy for evaluation of the climate shifts in the years 2013–2022. We propose two distinct approaches by GMT and R to process automatically geospatial datasets of diverse origin and types: the first (GMT) optimizes the cartographic workflow for plotting a series of climatic maps; the second (R) is applied for satellite image processing and automated unsupervised classification. We show that our scripting approach are well adapted to rapid and accurate processing of the multi-format geospatial datasets and enable high-quality cartographic visualization.

2. Study area

A sub-saharan African landlocked country situated in the southern Sahel (Fig. 1), Burkina Faso experiences extreme climatic hazards (Zougmoré et al., 2018). These vary from the extreme floods in Volta River Basin, one of the most vulnerable regions in West Africa to

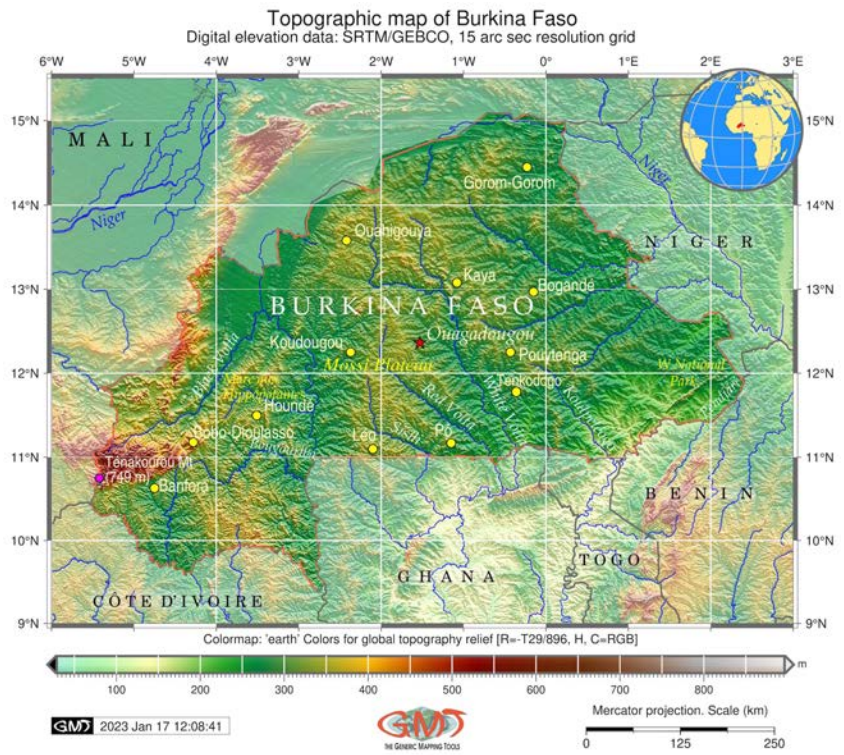

Fig. 1. Topographic map of Burkina Faso, West Africa. Mapping software: GMT scripting toolset. Data source: GEBCO/SRTM. Cartography: authors

hydrological disasters, desertification (Rochette, 1989; Rasmussen et al., 2001; Capozzi et al., 2018) and recurrent droughts (Reij et al., 2005; Kasei et al., 2010; Okafor et al., 2021) caused by the rise in annual temperatures and decreased runoff. The problems of climate change in sub-saharan Africa are largely discussed in many papers (Olsson, 1993; Waha et al., 2013; Webber et al., 2014; Azibo and Kimengsi, 2015; Waongo et al., 2015; Ayanlade et al., 2021; Ascott et al., 2022; Emediegwu et al., 2022). Major risks of climate change include the decline in precipitation and increase in annual temperatures. As a consequence, such trends results in changed vegetation patterns, deforestation and desertification in West Africa, and negatively affect food production in agricultural sector, both rainfed and irrigated crop yields (Calzadilla et al., 2013).

Climate change issues pose high risks to the vegetation sustainability, food security in mixed crop–livestock systems (Rigolot et al., 2017). The reported consequences of the climate impacts in Burkina Faso include changes in land cover types with detected increase in tree savannah, bare soils and agricultural lands, and decrease in woodland, gallery forest, shrub savannah and water areas (Dimobe et al., 2018). At the same time, the biodiversity loss indicate rapid climate shift and reflect changes in rainfall patterns, declining water balance and increased extreme climate events (Hannah et al., 2020). Besides climate factors, anthropogenic activities contribute to land degradation and deforestation

through agricultural lands expansion of croplands, which leads to the decrease of woody savannah and gallery forests in the country. For instance, previous studied (Gaisberger et al., 2017) mentioned overexploitation, overgrazing, fire, cotton production, mining activities, besides climate change, among the major threatening factors to existence of the selected vulnerable tree species in Burkina Faso. Other studies reported high susceptibility of the country to mini-droughts, heatwaves, torrential rainfalls, and extreme weather events (Sorgho et al., 2021). In turn, the issues of social consequences and adaptation strategies to climate change in Burkina Faso are discussed earlier (Offerle et al., 2005; Ouedraogo et al., 2012).

Burkina Faso is one of the least developed countries in the world with the highest level of poverty. Its economy largely depends on the agriculture sector and the use of natural resources (Barro et al., 2015). Therefore, maintaining environmental sustainability through monitoring and ecological analysis is important for development of this country. However, recent issues of climate change resulted in continuous degradation in the agricultural-pastoral potentialities of the country, caused by both the intensive use of resources (Vall et al., 2017) and climate change (Dimobe et al., 2022b). Common agricultural species mostly planted in semi-urban areas of Burkina Faso include sorghum, millet, maize and rice as the principal cereals (Arumugam et al., 2023; Séogo and Zahonogo, 2023). Examples of other agricultural products include tomatoes, lettuce, cabbage, beans, eggplants, etc. (Ouédraogo et al., 2019), typical for the individual small-scale farming households for subsistence farming. A moderate production of cotton (less than 1 t/ha) contributed to the development of traditional agrarian cropping systems in the savannah of Burkina Faso and remains a notable feature of its agricultural and development policies (Soumaré et al., 2021).

High exposure and low adaptive capacity to climate-related hazards require development of adaptive strategies in Burkina Faso with aim to control food management, secure agricultural production and maintain environmental sustainability (Daniel et al., 2013; Bunclark et al., 2018). Since the country is located in a tropical climate, is has two distinct seasons – severe dry season which lasts from November to May and wet rainy season from June to October (Ofori-Sarpong, 1987). The intense raining increases the quantity of the eroded soil which is greater during the rainy season (Sanou, 1993). As a result, the intra-seasonal variability in rainfall and precipitation controls soil and vegetation structure and the periods of agricultural and pastoral activities (Brons et al., 2000).

The increased drought periods and intensity threaten to crop systems and livelihoods of Burkinabè farmers and pose high risks to sustainable yield harvesting (Salter and Goode, 1967; Gbode et al., 2022; Sawadogo, 2022). Besides, the decrease of precipitation directly affects the soil structure and biochemistry of plants. For instance, high salinity of soil which increases during the periods of drought negatively affects the yields of maize, rice and other grain crops in Burkina Faso. Other consequences of climate change report variations in catchment hydrology and increased soil erosion, changes in evapotranspiration, water discharge and pattern of sedimentation (Op de Hipt et al., 2018; 2019).

The vegetation of Burkina Faso is controlled by the distribution of climate gradients, and includes the two major landscape types – the Sudanian with typical savannah,

open woodlands and gallery forests, and the Sahelian with dominated Acacia, steppe shrubs and scattered trees (Da, 2010). The carbon density in tree aboveground biomass is increasing significantly from the Sudano-Sahelian zone towards the Sudanian zone. It is also positively correlated with the mean annual precipitation, which proves that climatic variables directly affect the dendrometric parameters of trees (Balima et al., 2021). The Sahelian type of vegetation is distributed in the northern part of the country, according to the major topographic units with a latitudinal orientation of the dune belts (Ballouche, 1998). Accordingly, Burkina Faso consists of two major types of landscapes varying along the major topographic units. The major part of the country is presented by a flat relief and gentle variations between the elevations, slightly undulating landscape and occasional isolated hills (Nebie, 1993), while the contrasting southwest includes the sandstone plateau massif bordered by the cliffs located close to the border with Mali where the highest peak of the country, the Ténakourou, is located (Fig. 1). A traditional agricultural farming (millet and sorghum) is being cultivated around Mossi Plateau.

Variations in humidity and aridity over Burkina Faso is the most fundamental factor which limits crop production, lowers the biomass production and limits the distribution area of the selected plant species and trees (Adjonou et al., 2020; Dimobe et al., 2020). Since the degree of moisture depends on the two key parameters – precipitation and temperature – it naturally differs for the arid northern and semi-arid southern tropics of the country and thus contributes to the distribution of the different vegetation types.

Spatiotemporal variability in humidity and rainfall variability of Burkina Faso were studied previously (Oguntunde et al., 2006) with the historical analysis of the dynamics that showed the decrease in the humidity over the three decades of the past century with the 1968 being the wettest and 1983 – the driest year. Moreover, other similar studies which performed the long-term data analysis since 1950s (De Longueville et al., 2016) report changes in the rainfall pattern in Burkina Faso in the last over 60 years. These include a general decrease of the total rainfall periods, an increase of the average rainfall for the wet days and maximum consecutive dry days and a decrease of maximum consecutive wet days in Burkina Faso. Furthermore, Belemtougri et al. (2021) report the increase in the observed number of dry months per 49 gauging stations in Burkina Faso over 1955–1985, which is higher in the northern parts of the country where the Sahelian vegetation type is dominating, followed by the Sudano-Sahelian and Sudanian zone, respectively. This indicates the risk of droughts and desertification in the northern parts of Burkina Faso and shift in vegetation types.

Further, Biasutti (2019) notes that the intensity and frequency of rainfall in Sahel is connected to the global monsoon circulation which is susceptible to the effects from the remote oceans. Thus, warming the oceans and the Sahara changes the structure and position of the regional air circulation which determines seasonal rain accumulation. These processes well illustrate and explain the observed multidecadal variability in rainfall trends in the West Africa in general and in Burkina Faso in particular. Besides the retrospective climate modelling, the existing examples of the predictive climate prognosis Gaetani et al. (2020) indicated possible scenarios in the expected climate shift and precipitation change in the West Africa in the near future which may affect the vegetation patterns in the West Sahel region.

While drought and desertification are the consequences of the climate-related issues such as decrease in precipitation and rainfall intensity, the deforestation in Burkina Faso is mostly triggered by the anthropogenic factors. These include, for instance, the replacement of the natural forests by rangeland and croplands due to the increased demand for agricultural land (Etongo et al., 2015). Such patterns in land cover change largely change the landscape structure in natural ecosystems. Moreover, human-induced effects are aggravated by the intensive agricultural activities with the use of fertilizers by the Burkinabè farmers in the Sahelian rural areas (Tarchiani et al., 2021). It is noted previously that the extent of the vegetation types in Burkina Faso is mostly controlled by the two factors: naturals constraints from the geomorphology, soil and climatic setting that determine the extent of the ecozones, and the anthropogenic activities such as uncontrolled agricultural and pastoral practices that cause degradation of the vegetal coverage in case of uncontrolled livestock systems and farming (Bandre, 1993).

3. Materials and methods

3.1. Data

This study included various data used for mapping climate parameters and land cover types. The climatic maps are based on the use of the TerraClimate high-resolution dataset showing monthly climate parameters (Abatzoglou et al., 2018). The general topographic map showing study area and the extent of the Burkina Faso in regional and global scales are based on the GEBCO/SRTM raster grid (GEBCO, 2020). The satellite image analysis was based on the Landsat-8 OLI/TIRS scenes (USGS, 2015) for Burkina Faso in years 2013 and 2022 obtained from the USGS repository (https://earthexplorer.usgs.gov/) (Fig. 2).

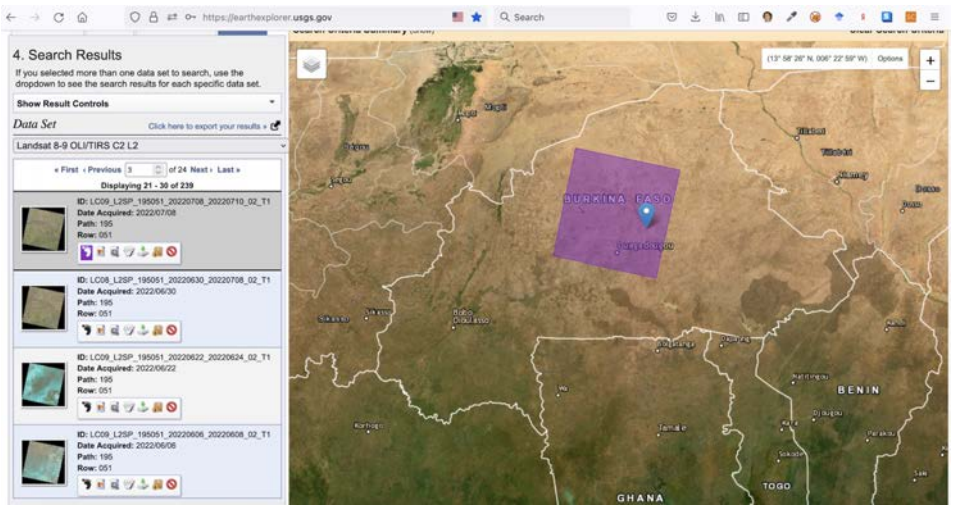

Fig. 2. Data capture from the EarthExplorer repository of the USGS: Landsat-8 OLI/TIRS satellite image, central Burkina Faso, Ouagadougou. Background image: ESRI World imagery

The detailed information on the Landsat imagery is available in the supporting technical documentation (USGS, 2022). The Landsat-8 OLI/TIRS images have 11 spectral bands with resolution of 30 meters in the multispectral channels. Using the Landsat OLI/TIRS images, we examined the difference in the land cover types and changes in vegetation patterns coverage between 2013 and 2022. The images were analysed using the K-means clustering algorithm of the unsupervised classification. The evaluation of the plant health conditions was computed using two vegetation indices for the 2013 and 2022: the Normalised Difference Vegetation Index (NDVI) and the Soil Adjusted Vegetation Index (SAVI).

3.2. Mapping climate parameters in GMT

A series of maps showing variations in the climatic and environmental parameters of Burkina Faso for years 2013 and 2022 has been plotted using the Generic Mapping Tools (Wessel et al., 2019) and the existing methods of the cartographic scripting described earlier (Lemenkova and Debeir, 2022a; 2022b). Mapping climate parameters in GMT was based on several GMT modules: gmtset, gmtdefaults, grdcut, makecpt, grdimage, psscale, grdcontour, psbasemap, gmtlogo, psconvert. The method of GMT works on a modular principle where each cartographic element is plotted using a line of code that controls its representation. Moreover, the execution of scripts is applicable for plotting the data of diverse source, formats and resolution. The main principles of the GMT cartographic methods are described below in details.

First, we refer to the map extent and spatial location as the inevitable definition of map. The target area was clipped using the coordinates (-6°W -3°W, 9°N–15.5°) from the global raster in NetCDF format using the 'grdcut' module for the area of Burkina Faso: "gmt grdcut TerraClimate_aet_2013.nc -R-6/3/9/15.5 -Gbf_aet2013.nc". The spatial extent is provided in the flag '-R' with defined coordinates extent in WESN extent. Using GDAL, we extract the necessary metadata from the file by '-stats bf_aet2013.nc' and define a colour palette according to the extreme values in the data range: "gmt makecpt -C20_hue_sat_light2.cpt -V -T0/74/1 -Ic > pauline.cpt".

The image is then visualised using the 'grdimage' module of GMT with the defined parameters of the spatial extent (-R), projection (-JM6.5i), the effects of the illumination on the map (-I+a15+ne0.75) and selected auxiliary features: '-X' defining the offset, and '-t25' defining the 25% transparency of the background image: "gmt grdimage bf_aet2013.nc -Cpauline.cpt -R-6/3/9/15.5 -JM6.5i -I+a15+ne0.75 -Xc -t25 -P -K > $ps". Plotting the isolines is one of the most widely used of all cartographic techniques: it visualizes the constant values of the target variables and enables to analyse the additive relationships between the variables by comparison of several maps if plotted for the same spatial extent. It is a most widely used element on topographic maps, but is also applied in climatic maps to visualise spatial variations in data values, e.g., temperature or evapotranspiration, which helps in the analysis of dynamics. Adding the isolines was done using the 'grdcontour' module of GMT as follows: "gmt grdcontour bf_aet2013.nc -R -J -C6 -A6 -Wthin,coral4 -O -K ≫ $ps".

The background geographic elements, such as coastlines, country borders and rivers were plotted on the map using the 'pscoast' module with defined the representation of lines as follows: "gmt pscoast -R -J -P -Ia/thinner,blue -Na -N1/thickest,white -W0.1p -Df -O -K ≫ $ps". To highlight the study area for a better contrast against the background, a technique of clipping was applied using the 'psclip' module. This enabled to plot a map within the masked area for a better contrast against the neighbouring countries by the following code: "gmt psclip -R-6/3/9/15.5 -JM6.5i BurkinaFaso.txt -O -K ≫ $ps". A grid added on a map is used for spatial interpretation of values and identification of their locations. Plotting a grid was performed using a drawn network of the major Eastings and Northings and evenly spaced auxiliary horizontal and vertical lines by module 'psbasemap': "gmt psbasemap -R -J -MAP_FRAME_AXES=WEsN –FORMAT_GEO_MAP=ddd:mm:ssF -Bpxg2f1a1 -Bpyg2f1a1 -Bsxg2 -Bsyg1 -B+t "AET (Actual Evapotranspiration) in Burkina Faso (2013)" -O -K ≫ $ps.

It is crucial to add colour legends on the maps for readability and correct perception of values. The colour legend was plotted on each of the maps using the 'psscale' module of GMT as follows: "gmt psscale -Dg-6.0/8.4+w16.0c/0.15i+h+o0.3/0i+ml+e -R -J -Cpauline.cpt -Bg5f0.5a10+l"Colormap palette: < ... >" -I0.2 -By+l"mm" -O -K ≫ $ps". The final output of the raster file was converted to the high resolution image using the GhostScript by the 'psconvert' module of GMT as follows: "gmt psconvert BF_aet_2013.ps -A0.5c -E720 -Tj -Z". The general principle of GMT described above was applied to plotting all the presented climatic and topographic maps using scripts that contained all the sequential lines of code with the parameters defined in commands, as demonstrated above. Each plotted map was executed from a corresponding script for visualising climate parameters for 2013 and 2022.

3.3. Image processing in R

The satellite image processing was performed to evaluate land cover changes and shift in patterns of the vegetation coverage in a selected area of Burkina Faso using the libraries of R language (R Core Team, 2022). The methodology of the satellite image processing in R is based on the existing workflow (Lemenkova and Debeir, 2022c; 2022d). The main components of the R scripts include libraries (terra, raster) and auxiliary packages such as 'RColorBrewer', 'graphics', and 'rgdal'. The 'rgdal' library was used to handle spatial data by integrating R with Geospatial Data Abstraction Library (GDAL) (URL: https://gdal.org/) for processing various spatial data formats, including the GeoTIFF. The 'rgdal' was used to apply the GDAL functionality to read the GeoTIFF files into computer memory, then passes these files to the libraries of R. The import, access and conversion of raster datasets to geospatial format were further processed by the RStudio desktop.

The calculation of the Normalized Difference Vegetation Index (NDVI) for the years 2013 and 2022 of the target area of Burkina Faso was performed in RStudio using the codes presented in appendix A1. The presented script is for the image of 2013. Likewise, this code was applied for the year 2022 with adjusted colour palette from the RColorBrewer brewer.pal(11, "Spectral") for the bands of the Landsat image

LC08_L2SP_195051_20220513_20220519_02_T1. The calculation of the Soil Adjusted Vegetation Index (SAVI) for the target area of Burkina Faso was performed in RStudio using the code presented in appendix A2. SAVI Computation with the example of 2013. The code was adjusted for the other Landsat image on 2022. The unsupervised classification for both years (2013 and 2022) was performed using the code available in the appendix A3. Unsupervised Classification and results listed in the appendix for both cases (2013 and 2022).

The major steps included first stacking a collection of the objects from the RasterLayer class which were initially stored in the Landsat bands. Since the raster files have the same spatial extent and resolution for the multi-spectral bands (except for thermal band which was not used for classification in this case), a stack of these files was created using the RasterStack function of R in 'raster' library. Thus, the RasterStack was formed using the separate Landsat OLI/TIRS bands as layers. Once it was created, a RasterBrick was made on the next step as a multi-layer raster object. This matrix was used further for clustering performed as an unsupervised classification of the two images. Its attributes are listed in the code snippet above showing the coordinate extent, resolution, dimensions and other metadata. Afterwards, the clustering was done using the 'unsuperClass' command of the 'raster' library.

The ten classes of the land cover types were selected based on the existing classification of the dominating land cover classes in Burkina Faso performed in the Land Cover Land Use project by the Food and Agriculture Organization of the United Nations (FAO) (URL: https://data.apps.fao.org/catalog/organization/fao-land-cover-land-use) with the available dataset (URL: https://data.apps.fao.org/catalog/iso/d5acf3e9-5f60-4338-8a7d-4dfe36acb7d0) as well as the classification supported by the United States Geological Survey (USGS) (URL: https://eros.usgs.gov/westafrica/land-cover/land-use-land-cover-and-trends-burkina-faso). The extended classification covering the whole country was modified and adopted according to the current extent of the study area located in the central part of the country. As a result, the following land cover classes were defined: 1) 'bare soil', 2) 'irrigated agricultural areas: cereals and legumes', 3) 'water areas and wetlands', 4) 'shrub lands', 5) 'savannah sahélienne' (sahelian short grass savannah), 6) 'savannah soudanienne', 7) 'steppe', 8) 'gallery forests and riparian forests', 9) 'forests', 10) 'urban settlements'. The computed results are reported in the appendices.

4. Results and discussion

In this section, a comprehensive description and analysis of the climatic data obtained from the TerraClimate dataset for Burkina Faso is provided both for 2013 and 2022. Furthermore, the changes in the parameters in the spatio-temporal extent are compared with regard to the geographic setting of the country. In Figure 3, the variations in minimal annual temperature over Burkina Faso for 2013 and 2022 obtained from the interpolated data from surface observations are shown.

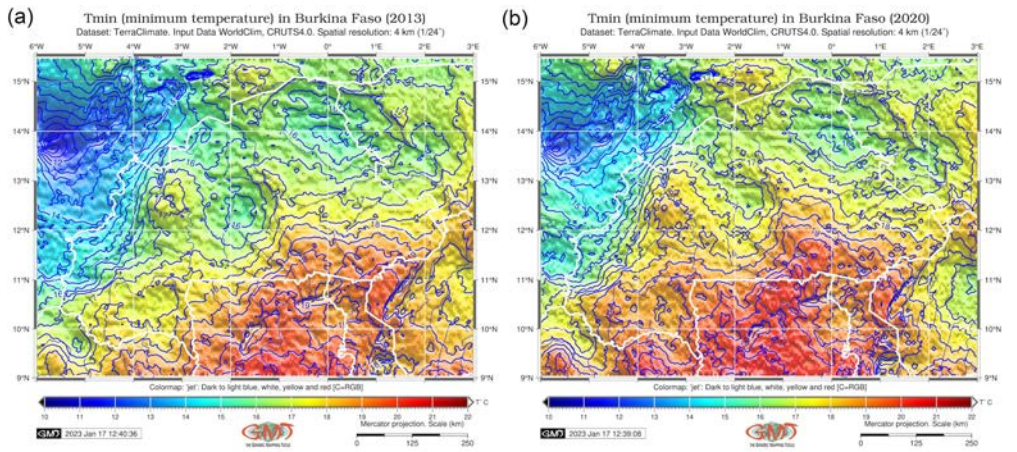

Fig. 3. Minimum temperature for Burkina Faso in (a) 2013 and (b) 2020

The data extent for 2013 ranges from 10.47°C to 20.56°C, while the data for 2022 has the extent from 11.70°C to 21.20°C which clearly shows the increase of the temperature on 1°C over 9 years. The interannual variability in maximal temperature ranging from 27.78°C to 37.14°C in 2013 against 28.20°C to 37.00°C in 2020 is compared with spatial variability in topography of Burkina Faso at regional scale (Fig. 4).

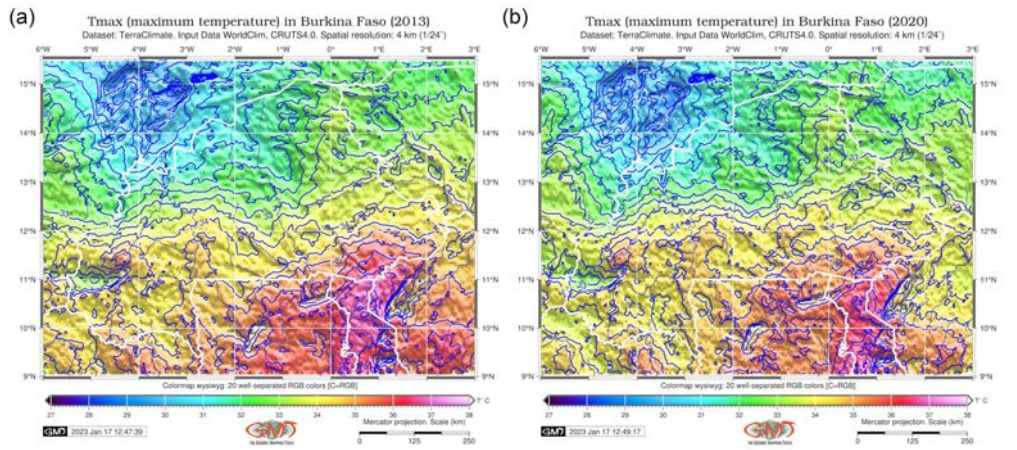

Fig. 4. Maximum temperature for Burkina Faso in (a) 2013 and (b) 2020

The data from from the TerraClimate show an association with the orographic pattern of the Mossi Plateau and the Ténakourou Mount. Thus, the areas of lower values in temperature are contoured by the isolines in Figure 4 which correlate with the topography of the country. This proves that the topography has an impact on the precipitation pattern in the mountainous regions. The same trend is clearly visible when compared the region in the south-western part of the country (Ténakourou Mount) where the temperatures

are lower than the values in the surrounding areas. This further illustrates the effects of the topography on climate variations and temperature variations. The analysis of the dynamics of soil moisture over the country (Fig. 5) shows that in 2013 the maximal values were 172.10 mm/m with a mean of 31.66 mm/m, while in 2022 the maximal value is only 150.40 mm/m with a mean of 27.92 mm/m, showing the decrease in soil moisture and the increase in dry lands in Burkina Faso over the recent 9 years. This well correlates with the data on the potential evapotranspiration (Fig. 6).

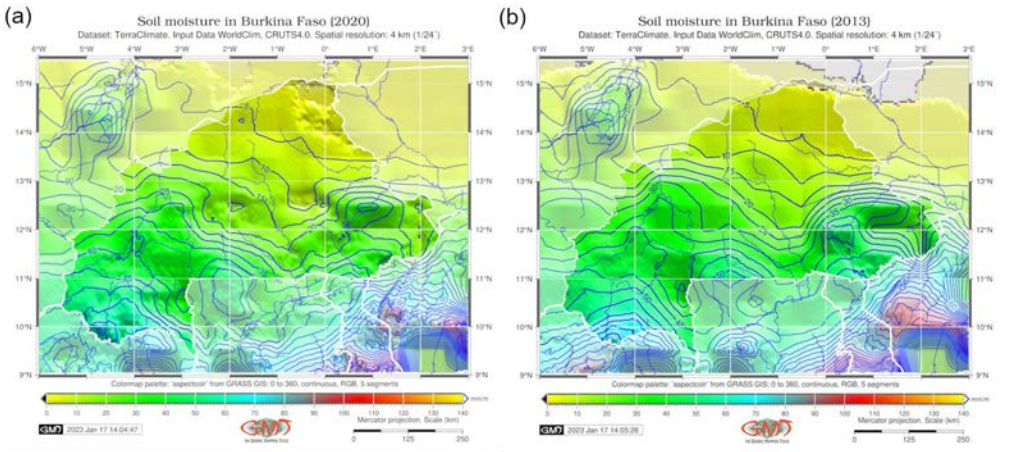

Fig. 5. Soil moisture in Burkina Faso in (a) 2013 and (b) 2020

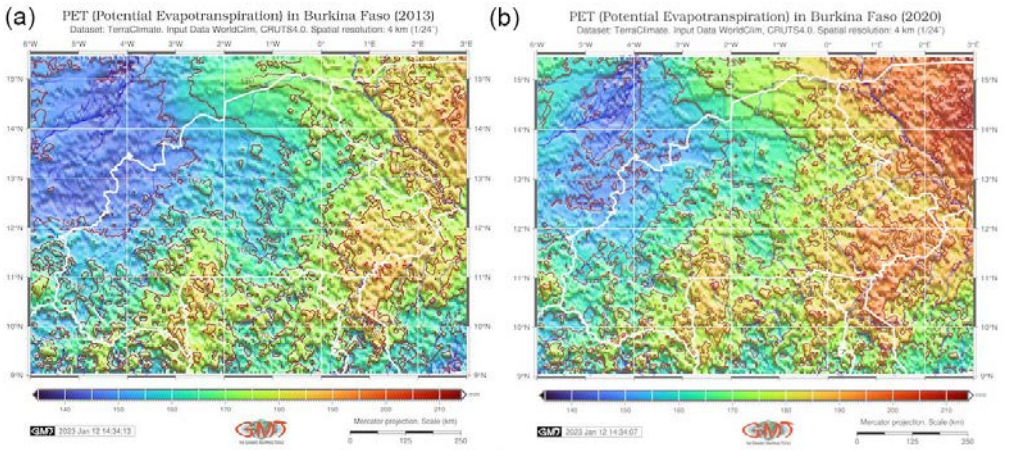

Fig. 6. Potential evapotranspiration (PET) in Burkina Faso in (a) 2013 and (b) 2020

The analysis of the potential evapotranspiration (Fig. 6) indicates the measure of potential water loss related to the dryness and temperature. Thus, the analysis of data on 2013 indicate the actual range from 135.40 to 197.50, while the 2022 year shows the increased data range diapason ranging from 139.00 to 214.90.

The data on actual evapotranspiration over Burkina Faso (Fig. 7) range from 0 to 76.10 in 2013, while decrease up to 74.30 as the maximal values in 2022, which shows the decrease in the liquid water supply and the utilized soil water that results in the changed values of the actual evapotranspiration. Thus, the decrease in liquid water supply necessarily results in lower values of actual evapotranspiration. The values of Vapour Pressure Deficit (VPD) for Burkina Faso (Fig. 8) range from the interval 2.18 to 3.53 kPa in 2013 to an interval from 2.19 to 3.38 kPa in 2022. Such variations showing the narrower range in recent years can be explained as follows. Since the VPD is an auxiliary data received in the original dataset using data for precipitation, monthly maximum and minimum temperature, and vapour pressure, the variations in VPD demonstrate changes related to these climatic parameters.

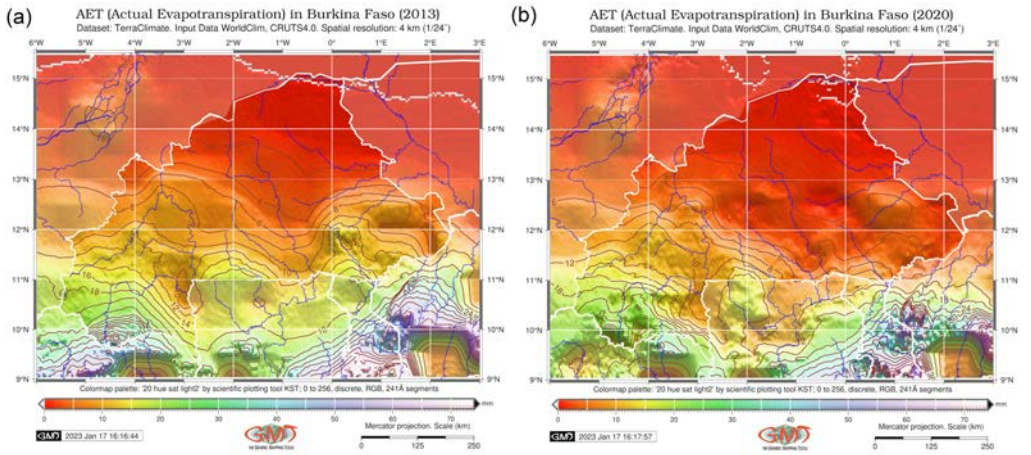

Fig. 7. Actual evapotranspiration (AET) in Burkina Faso in (a) 2013 and (b) 2020

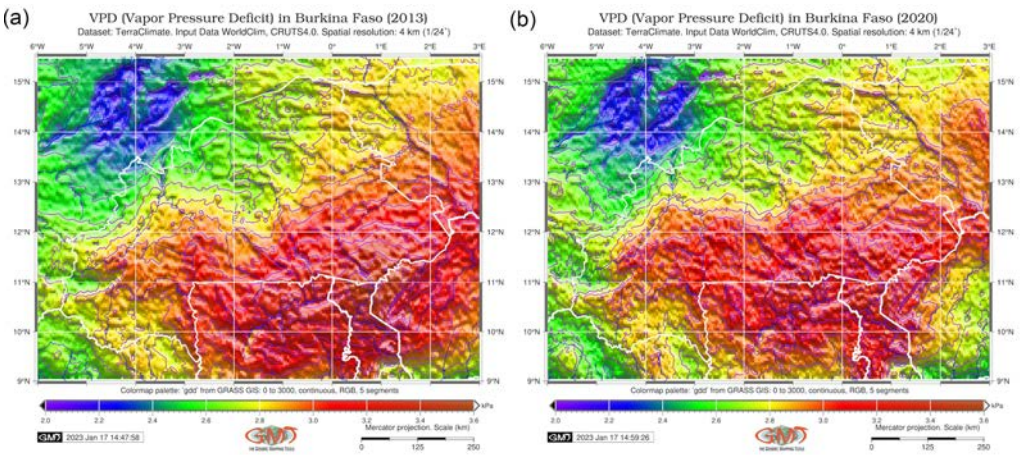

Fig. 8. Vapour Pressure Deficit (VPD) in Burkina Faso in (a) 2013 and (b) 2020

The data on Vapour Pressure (VAP) in Burkina Faso (Fig. 9) show the range from 0.45 kPa to 1.44 kPa in 2013, while a shift is notable in 2022 to the range from 0.48 kPa to 1.41 kPa. Such a narrower diapason of data extent also correlates with the variables of air temperature, pressure of air, hydrological precipitation process and the porosity of soil. Likewise, the downward surface shortwave radiation in Burkina Faso (Fig. 10) demonstrates changes from the 203.50 to 233.10 Wm-2 in 2013 to the intensification of data in a slightly narrower range from 207.20 to 233.50 Wm-2 in 2022 that reflects the shift in the related essential climate variable – the intensity of solar energy as a source of short wave radiation.

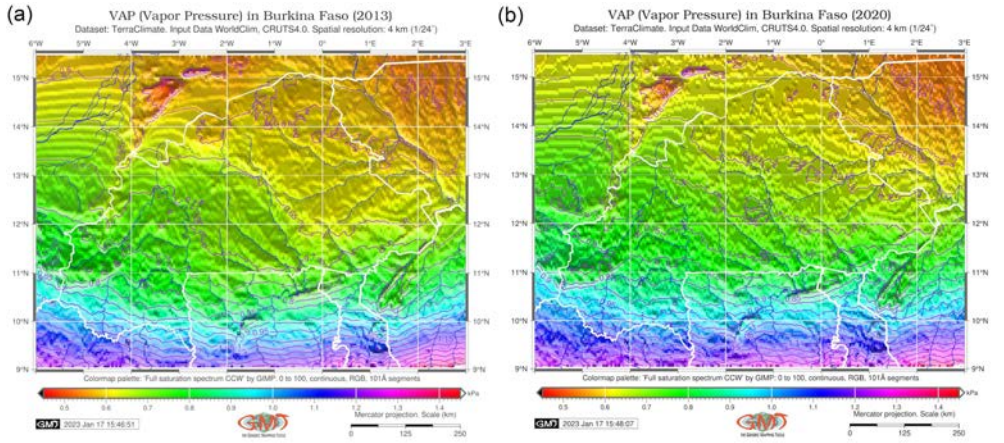

Fig. 9. Vapour Pressure (VAP) in Burkina Faso in (a) 2013 and (b) 2020

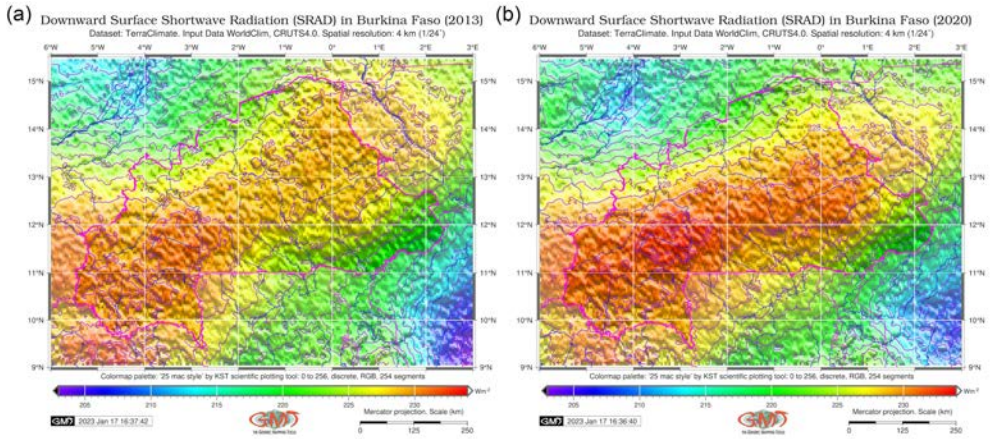

Fig. 10. Downward Surface Shortwave Radiation (SRAD) in Burkina Faso in (a) 2013 and (b) 2020

The data on average annual wind speed for Burkina Faso (Fig. 11) shows the extent in data from the minimal at 1.70 m/s to the maximal at 3.38 m/s with a mean of 2.31 m/s in 2013. In 2022, the data range shifts to a wider difference in values from 1.60 m/s to

3.89 m/s (Fig. 11) showing a larger range of the extreme wind speed. This well correlates with the increase of the climatic extreme events, as discussed earlier. The variations in values of the Palmer Drought Severity Index (PDSI) in Burkina Faso (Fig. 12) shows the change in the data range from –8.32, to a maximum of 7.03, with a mean of 2.01 in 2013, while a more recent data show the minimum at –7.20, maximum at 5.92 and a mean of –2.20 in 2022. The narrower range in the PDSI values indicates a trend to the drought that supports recent observations on climate change in Burkina Faso with related forest drought stress, as also observed in other regions of the West Africa.

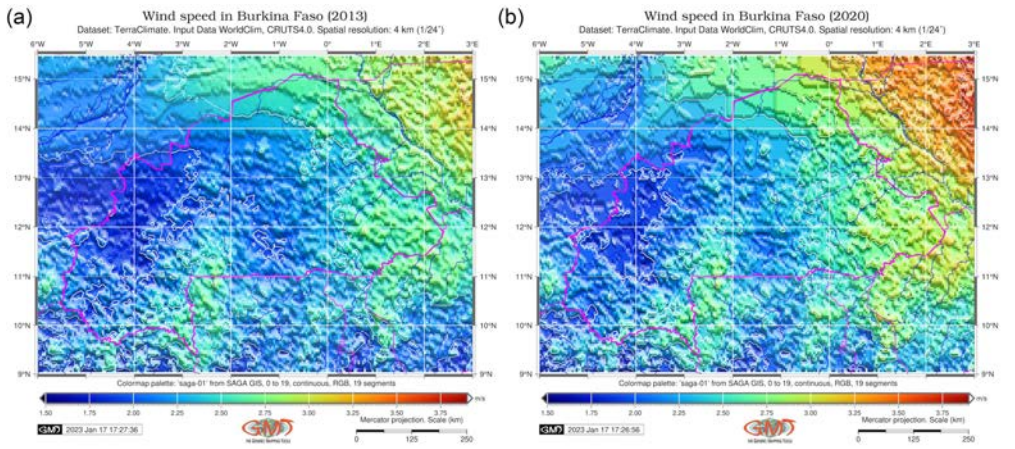

Fig. 11. Average wind speed in Burkina Faso in (a) 2013 and (b) 2020

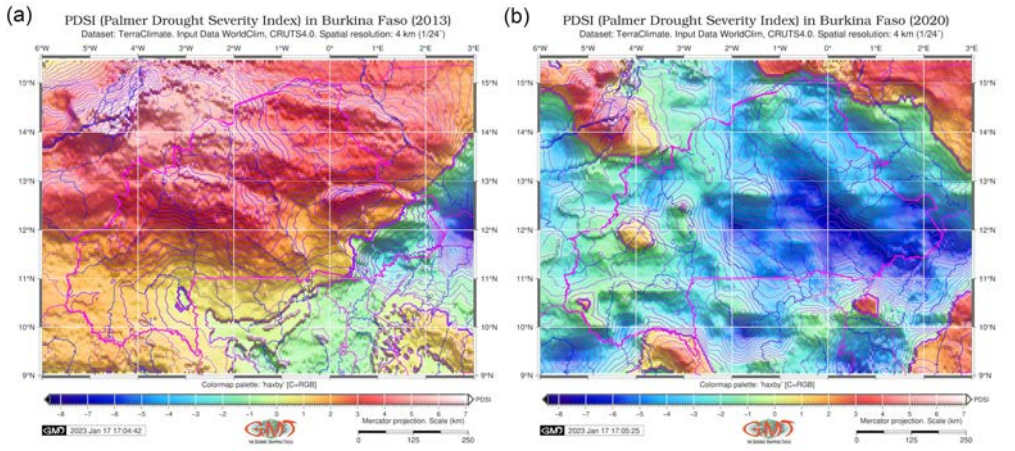

Fig. 12. PDSI (Palmer Drought Severity Index) in Burkina Faso in (a) 2013 and (b) 2020

The Normalized Difference Vegetation Index (NDVI) is used to compute the values of the vegetation greenness using a classifier-based approach in R language (Fig. 13). In this approach, the basis classes of the NDVI values are defined directly as the categories

of the vegetation vigour based on the spectral reflectance of the plants in Bands 4 and 5 which correspond to the Red and NIR spectral channels in the Landsat OLI/TIRS images. These bands are used to indicate vegetation health through the greenness expressed as the amount of the chlorophyll content in leaves detectable by the NDVI through the Red/NIR combination of bands. Thus, healthy vegetation has values of near +1, while medium values are typical for the grassy or shrubby savannah; lower values show sparse vegetation, while negative values indicate water areas.

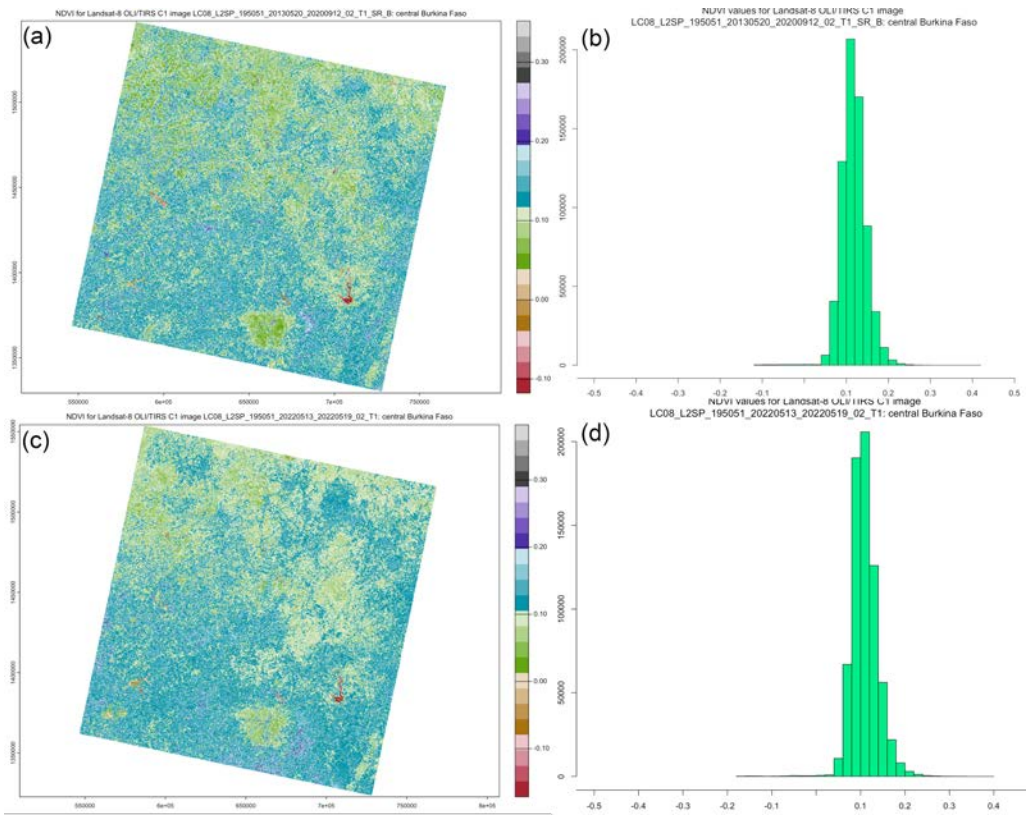

Fig. 13. NDVI (a, c) and histogram (b, d) for Burkina Faso in 2013 (a, b) and 2022 (c, d)

The algorithm of computing the NDVI by R is trained to recognize the categories of high NDVI values that correspond to the green and health vegetation typical for forest areas. Specifically for Burkina Faso, the majority of the NDVI values for the examined images show values typical for savannah, that is, around 0.2. A slight decrease in values is notable when comparing the images for 2013 and 2022 which might indicate the processes of desertification (Fig. 13).

The Soil-Adjusted Vegetation Index (SAVI) method implements the soil-brightness correction factor to lessen the effects from the soil brightness (Fig. 14). The use of SAVI is especially actual for the northern region of Burkina Faso in southern Sahara Desert where very sparsely vegetated areas are dominated with only sporadic trees. The SAVI

index is defined as a difference between the NIR and Red bands in the Landsat OLI/TIRS images adjusted to the soil brightness correction factor (L) set as 1/2 to be suitable for the most land cover types. For the two examined Landsat OLI/TIRS images of the Burkina Faso for 2013 and 2022, the majority of SAVI values lie in the range from 0.08 to 0.20 in 2013, while for the 2022 the values shift towards the range of 0.06 to 0.18 showing a slight decrease in values typical for healthy vegetation (Fig. 14).

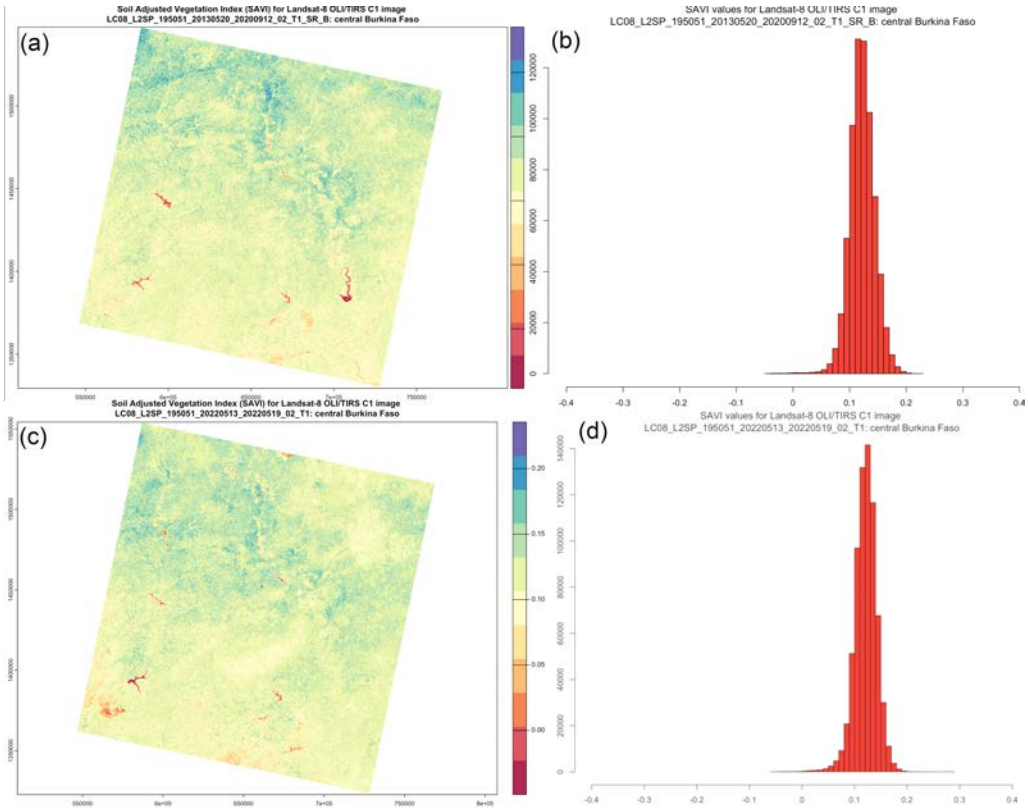

Fig. 14. SAVI (a, c) and histogram (b, d) for Burkina Faso in 2013 (a, b) and 2022 (c, d)

The land cover changes and dynamics of deforestation in Burkina Faso were compared for the year 2013 (Fig. 15) and 2022 (Fig. 16) using the analysis of clustering results. While R employs cluster centroids to render the classifier nonlinear and accurate, here the non-labeled data are used for objectivity of clustering by adopting the explicit object features by a spectral reflectance of pixels on the images as representations of the land cover classes and landscape dynamics in Burkina Faso. The appendix B shows the results of the classifications of the Landsat OLI/TIRS images for each year with reported number of pixels in each of the 10 land cover classes.

The clustering method in R was introduced by the algorithm in 'RStoolbox' library. The algorithm learns a distance between the cluster centroids and assigns each pixels to the target class among the available 10 classes. The assignment of pixels is based on

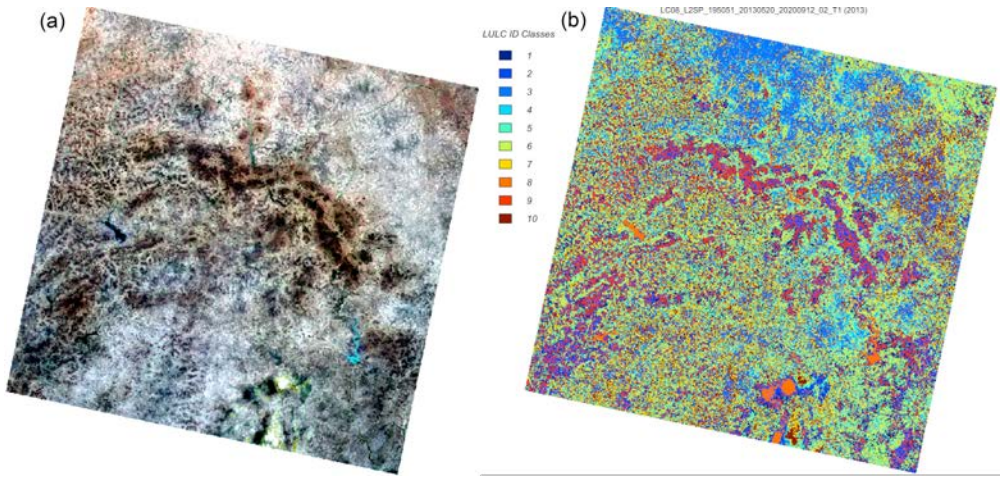

Fig. 15. Analysis of land use cover (LULC) types Burkina Faso. Landsat-8 OLI/TIRS color composites (4-3-2) (a) and clusters of LULC based on unsupervised classification (b) for 2013

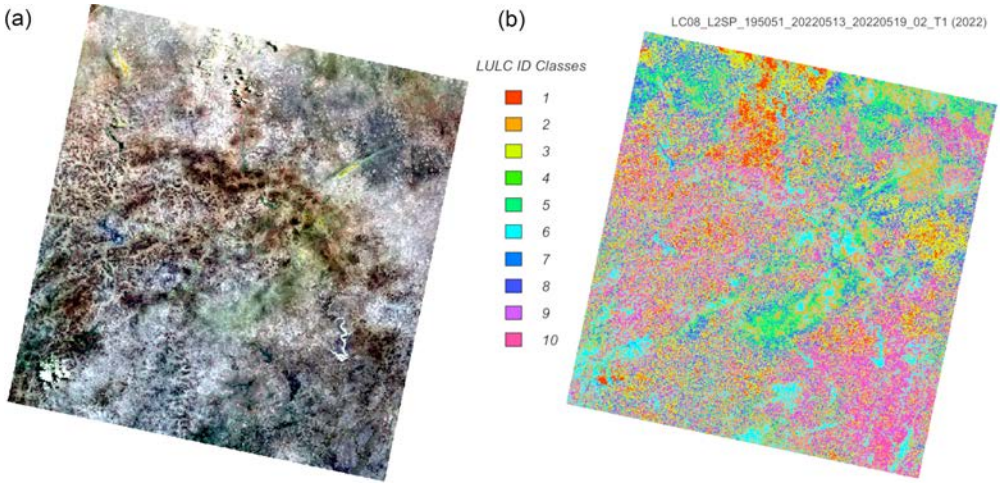

Fig. 16. Analysis of land use cover (LULC) types in Burkina Faso: Landsat-8 OLI/TIRS color composites (4-3-2) (a) and clusters of LULC based on the unsupervised classification by K-means clustering (b) for 2022

the measuring a distance between the pixel value and the centroid of each cluster in the observation dataset. The major classes include the following land cover types typical for Burkina Faso: 1) 'bare soil', 2) 'irrigated agricultural areas: cereals and legumes', 3) 'water areas and wetlands', 4) 'shrub lands', 5) 'savannah sahélienne' (sahelian short grass savannah), 6) 'savannah soudanienne', 7) 'steppe', 8) 'gallery forests and riparian forests', 9) 'forests', 10) 'urban settlements'. The difference in the land cover classes is mapped for 2013 (Fig. 15) and 2022 (Fig. 16). The computed difference in each land cover class is reported in the appendix for images of 2013 and 2022.

5. Conclusion

In this paper, we presented an investigation of the climate-environmental relationships in Burkina Faso, West Africa which integrated remote sensing and climate datasets. The study showed an overview of the climate issues and environmental challenges in Burkina Faso, with relation to the agricultural system of the country. To reveal the links between the climate-related processes and environmental responses, the advanced mapping tools is essential. To this end, an efficient scripting methods of the GMT and R were applied for mapping climate-environmental parameters as an integrated tool for accurate and data visualization. The programming techniques were applied using for automated workflow of the satellite image processing with a case of geospatial libraries of R language. The obtained results and observed variations in environmental parameters in Burkina Faso are discussed at regional scale and at local scale with an enlarged fragment of the study area. The effectiveness of scripting techniques for cartographic workflow was demonstrated with respect to mapping climate and environmental parameters and image processing. The results included computed vegetation indices NDVI and SAVI and classified land cover changes over the territory of Burkina Faso. For comparison of the environmental changes, the maps were presented for the years 2013-2022.

To handle complex environmental scenarios encountered in the Burkina Faso due to the climate change, we propose a pairwise comparative mapping and image processing of the data on years 2013 and 2020 for each evaluated climatic and environmental parameter. The presented data visualization by scripts is a semi-automated mapping process run through a console which is interleaved with adjustment of selected parameters in script for each map according to the data range and extend.

In this work, we proposed a scripting approach for remotely sensed geospatial data processing aimed at mapping climate and land cover variables by GMT and R. It is built on a console-based method of data handling that uses a syntax of programming language for visualization of spatial datasets. Therefore, prewritten codes are sufficient enough to achieve a high speed for plotting data (about/less than a second for map visualization) and a high accuracy of the final outputs as a series of maps. Practical issues of the used methodology include the advantages of the open source tools. While the commercial GIS, besides being expensive, sometimes include the unfixed bugs and restricted functionality, and create a certain dependency of a user on software vendors, open source tools such as GMT and R are available in full functionality with regular updates of the modified versions.

Further, the geospatial representation approach offered by the GMT scripting toolset and R language returns an effective series of maps showing target environmental parameters over the area of Burkina Faso, compared pairwise for 2013 and 2022 for the analysis of the environmental dynamics. Extensive experiments with scripts on TerraClimate and the Landsat OLI/TIRS satellite images demonstrate that our method is effective and can be extended on a wider range of complex environmental scenarios in West Africa. Moreover, practical issues including the data analysis and comparison of the dynamics of climate variables and vegetation coverage derived from the remote sensing data are handled under our unified GMT-R framework. Using the GMT and R tools, the image

processing and mapping were implemented for climate and environmental analysis of the Burkina Faso. The GMT was used for cartographic data processing and mapping the climate parameters of the TerraClimate dataset. The scripting method of R is robust to processing data using unsupervised learning algorithm of k-means clustering that was used for land cover classification. Libraries of R are capable of efficient image processing for vegetation mapping and environmental analysis. The partitioning of pixels on the satellite images into the defined land cover classes categorized into groups according to the similarity of their spectral reflectances, and demonstrated the difference of land cover classes for 2013 and 2022 in Burkina Faso. Using R and GMT scripts, we are able to incorporate the spatial contiguity of the geospatial continuum fields and analyze their variability over space, thereby fully realizing the potential of the advanced scripting cartographic methods.

Appendix

Appendix A. R scripts used for satellite image processing

A1. NDVI Computation

```
library(terra)
install.packages("pals")
library(pals)
library(RColorBrewer)
#comment:"/Users/USERNAME/..." is a sample path for the authors' folder structure which should be modified when reusing.
setwd("/Users/USERNAME/Documents/R/52_Image_Processing/
LC08_L2SP_195051_20130520_20200912_02_T1")
# 1. NDVI = (NIR - R) / (NIR + R), i.e., NDVI = (Band 5 – Band 4) / (Band 5 + Band 4).
vi <- function(img, k, i) {
  bk <- img[[k]]
  bi <- img[[i]]
  vi <- (bk - bi) / (bk + bi)
  return(vi)}
# For Landsat NIR = 5, red = 4.
filenames <- paste0('LC08_L2SP_195051_20130520_20200912_02_T1_SR_B', 1:7, ".tif")
filenames
landsat <- rast(filenames)
landsat
ndvi <- vi(landsat, 5, 4)
# defining color palette
colors <- stepped()
plot(ndvi, col = colors, font.main = 1, main = "NDVI for Landsat-8 OLI/TIRS C1 image
LC08_L2SP_195051_20130520_20200912_02_T1_SR_B: central Burkina Faso", cex.main=0.9)
# Plotting the histogram of the NDVI
hist(ndvi, font.main = 1, main = "NDVI values for Landsat-8 OLI/TIRS C1 image
\nLC08_L2SP_195051_20130520_20200912_02_T1_SR_B: central Burkina Faso",
xlab = "NDVI", ylab= "Frequency", col = "springgreen2", xlim = c(-0.5, 0.5),
breaks = 30, xaxt = "n") axis(side=1, at = seq(-0.6, 0.5, 0.1),
labels = seq(-0.6, 0.5, 0.1))
```

A2. SAVI Computation

```
SAVI = ((Band 5 – Band 4) / (Band 5 + Band 4 + 0.5)) * (1.5).
savi_fun = function(nir, red){
 ((nir - red) / (nir + red + 0.5)) * 1.5}
savi = lapp(landsat[[c(4, 3)]],
     fun = savi_fun)
plot(savi, col = brewer.pal(11, "Spectral"), font.main = 2, main =
"Soil Adjusted Vegetation Index (SAVI) for Landsat-8 OLI/TIRS C1 image
\nLC08_L2SP_195051_20130520_20200912_02_T1_SR_B:
central Burkina Faso", cex.main=1.0)
hist(savi, font.main = 1, main = "SAVI values for Landsat-8 OLI/TIRS C1 image
\nLC08_L2SP_195051_20130520_20200912_02_T1_SR_B: central Burkina Faso",
xlab = "SAVI", ylab= "Frequency", col = "firebrick2", xlim = c(-0.4, 0.4),
breaks = 30, xaxt = "n") axis(side=1, at = seq(-0.4, 0.4, 0.1),
labels = seq(-0.4, 0.4, 0.1))
```

The same code was repeated for the year 2022 for the files of the Landsat-8 OLI/TIRS image LC08_L2SP_195051_20220513_20220519_02_T1.

A3. Unsupervised Classification

```
library(rgdal)
library(raster)
library(terra)
library(RColorBrewer)
library(pals)
library(colorspace)
library(RStoolbox)
library(graphics)
#comment:"/Users/USERNAME/..." is a sample path for the authors' folder structure which
should be modified to the actual working folder when reusing.
setwd("/Users/USERNAME/Documents/R/52_Image_Processing/
     LC08_L2SP_195051_20130520_20200912_02_T1")
Landsat_BF2013 <- list.files("/Users/USERNAME/Documents/R/
52_Image_Processing/LC08_L2SP_195051_20130520_20200912_02_T1")
list.files()
[1] "LC08_L2SP_195051_20130520_20200912_02_T1_SR_B1.TIF"
[2] "LC08_L2SP_195051_20130520_20200912_02_T1_SR_B2.TIF"
[3] "LC08_L2SP_195051_20130520_20200912_02_T1_SR_B3.TIF"
[4] "LC08_L2SP_195051_20130520_20200912_02_T1_SR_B4.TIF"
[5] "LC08_L2SP_195051_20130520_20200912_02_T1_SR_B5.TIF"
[6] "LC08_L2SP_195051_20130520_20200912_02_T1_SR_B6.TIF"
[7] "LC08_L2SP_195051_20130520_20200912_02_T1_SR_B7.TIF"
Landsat_BF2013_stack <- stack(Landsat_BF2013)
Landsat_BF2013_brick <- brick(Landsat_BF2013_stack)
Landsat_BF2013_brick
class    : RasterBrick
dimensions  : 7281, 7471, 54396351, 7 (nrow, ncol, ncell, nlayers)
resolution   : 30, 30 (x, y)
extent       : 545085, 769215, 1329285, 1547715 (xmin, xmax, ymin, ymax)
crs    : +proj=utm +zone=30 +datum=WGS84 +units=m+no_defs
```

source : r_tmp_2023-01-22_145640_95034_42547.grd
names : LC08_L2SP//2_T1_SR_B1, LC08_L2SP//2_T1_SR_B2,
LC08_L2SP//2_T1_SR_B3, LC08_L2SP//2_T1_SR_B4, LC08_L2SP//
2_T1_SR_B5, LC08_L2SP//2_T1_SR_B6,LC08_L2SP//2_T1_SR_B7
min values : 1527, 2952, 8310, 9634, 9791, 9470, 8779
max values : 33177, 35035, 42211, 45735, 48008, 56959, 59325
set.seed(25)
unC <- unsuperClass(Landsat_BF2013_brick, nSamples = 100, nClasses = 10, nStarts = 5)
unC

Appendix B. Results of the computed unsupervised classification (2013): clustering of the Landsat-8 OLI/TIRS image (2013)

********** Model **********
$model
K-means clustering with 10 clusters of sizes
12, 4, 12, 11, 18, 8, 14, 1, 8, 12
Cluster centroids:
 LC08_L2SP_195051_20130520_20200912_02_T1_SR_B1
1 9599.417
2 9099.500
3 10990.750
4 10468.000
5 9708.778
6 10022.250
7 9971.857
8 8644.000
9 9177.250
10 10560.250
 LC08_L2SP_195051_20130520_20200912_02_T1_SR_B2
1 10457.250
2 9865.500
3 12085.750
4 11398.000
5 10611.333
6 10902.500
7 10907.714
8 9627.000
9 9930.375
10 11580.917
 LC08_L2SP_195051_20130520_20200912_02_T1_SR_B3
1 12754.50
2 11941.00
3 15290.75
4 14130.91
5 13067.61
6 13447.00
7 13600.07
8 11957.00

9 11989.38
10 14613.92
LC08_L2SP_195051_20130520_20200912_02_T1_SR_B4
1 14807.42
2 13264.25
3 18427.08
4 16949.27
5 15231.33
6 16301.62
7 16040.43
8 13009.00
9 13817.12
10 17467.50
LC08_L2SP_195051_20130520_20200912_02_T1_SR_B5
1 18633.08
2 17763.50
3 22331.33
4 21115.36
5 19915.61
6 20343.62
7 20832.00
8 15951.00
9 17179.50
10 21738.67
LC08_L2SP_195051_20130520_20200912_02_T1_SR_B6
1 22669.83
2 19796.75
3 26822.83
4 26232.27
5 23172.50
6 25491.88
7 24233.14
8 16494.00
9 21307.12
10 25430.42
LC08_L2SP_195051_20130520_20200912_02_T1_SR_B7
1 18583.08
2 15760.00
3 22718.25
4 22171.91
5 19110.56
6 21400.00
7 20214.29
8 14339.00
9 17072.25
10 21076.58
Within cluster sum of squares by cluster:
[1] 16849325 7559750 11280118 10249179 31001897 9960346 14629344 0 9426130
[10] 17899304

********** Map **********
$map
class : RasterLayer
dimensions : 7281, 7471, 54396351 (nrow, ncol, ncell)
resolution : 30, 30 (x, y)
extent : 545085, 769215, 1329285, 1547715 (xmin, xmax, ymin, ymax)
crs : +proj=utm +zone=30 +datum=WGS84 +units=m +no_defs
source : r_tmp_2023-01-22_145808_95034_17510.grd
names : class
values : 1, 10 (min, max)

Appendix C. Results of the computed unsupervised classification (2022): clustering of the Landsat-8 OLI/TIRS image (2022)

unsuperClass results
********** Model **********
$model
K-means clustering with 10 clusters of sizes 4, 9, 13, 1, 18, 8, 1, 20, 11, 1
Cluster centroids:

	LC08_L2SP_195051_20220513_20220519_02_T1_SR_B1
1	11011.750
2	9336.444
3	10578.769
4	4754.000
5	9667.111
6	8933.125
7	4468.000
8	10271.650
9	9573.818
10	9855.733

	LC08_L2SP_195051_20220513_20220519_02_T1_SR_B2
1	11976.25
2	10192.44
3	11707.31
4	7913.00
5	10677.00
6	9790.00
7	7616.00
8	11237.10
9	10389.82
10	10789.40

	LC08_L2SP_195051_20220513_20220519_02_T1_SR_B3
1	15083.25
2	12363.67
3	14619.31
4	14343.00
5	13239.39
6	11744.12

7 11846.00
8 13903.00
9 12660.73
10 13184.67
LC08_L2SP_195051_20220513_20220519_02_T1_SR_B4
1 18347.75
2 14332.78
3 17550.46
4 17431.00
5 15494.72
6 13494.00
7 14428.00
8 16494.15
9 15077.27
10 15543.13
LC08_L2SP_195051_20220513_20220519_02_T1_SR_B5
1 22078.00
2 17967.78
3 21226.54
4 20995.00
5 19791.06
6 16980.62
7 17511.00
8 20518.50
9 18044.82
10 19395.73
LC08_L2SP_195051_20220513_20220519_02_T1_SR_B6
1 26910.00
2 21401.00
3 24825.08
4 24269.00
5 22311.72
6 19593.88
7 18156.00
8 23698.45
9 22910.73
10 23910.80
LC08_L2SP_195051_20220513_20220519_02_T1_SR_B7
1 23312.50
2 17217.22
3 20677.92
4 20391.00
5 18186.56
6 16052.62
7 15714.00
8 19731.05
9 18731.36
10 19561.47
Within cluster sum of squares by cluster:

[1] 10243744 13359721 29109152 0 28575937 20311570 0 29155830 16295670
[10] 14514939
********** Map **********
$map
class : RasterLayer
dimensions : 7721, 7561, 58378481 (nrow, ncol, ncell)
resolution : 30, 30 (x, y)
extent : 545085, 771915, 1322685, 1554315 (xmin, xmax, ymin, ymax)
crs : +proj=utm +zone=30 +datum=WGS84 + units=m + no_defs
source : r_tmp_2023-01-22_155940_745_17510.grd
names : class
values : 1, 10 (min, max)

Author contributions

Conceptualization: O.D.; methodology and software: O.D., P.L.; writing original draft: P.L.; mapping, data processing and visualization: P.L.; validation: P.L.; writing after review and editing: P.L; supervision: O.D.; project administration: O.D.; funding acquisition: O.D.

Data availability statement

The satellite images used in this study are available from the USGS EarthExplorer repository (https://earthexplorer.usgs.gov/). The environmental data are obtained from TerraClimate (https://climate.northwestknowledge.net/TERRACLIMATE/index_directDownloads.php). The topographic data are available from GEBCO website in GeoTiff, Esri ASCII and NetCDF formats (https://www.gebco.net/data_and_products/gridded_bathymetry_data/).

Acknowledgements

We thank the three anonymous reviewers for the review of this paper and provided useful and detailed comments which improved the initial version of the manuscript. This project was supported by the Federal Public Planning Service Science Policy or Belgian Science Policy Office, Federal Science Policy – BELSPO (B2/202/P2/SEISMOSTORM).

References

Abatzoglou, J., Dobrowski, S., Parks, S. et al. (2018). TerraClimate, a high-resolution global dataset of monthly climate and climatic water balance from 1958–2015. *Sci. Data*, 5, 170191. DOI: 10.1038/sdata.2017.191.

Adjonou, K., Abotsi, K.E., Segla, K.N. et al. (2020). Vulnerability of African Rosewood (Pterocarpuserinaceus, Fabaceae) natural stands to climate change and implications for silviculture in West Africa. *Heliyon*, 6, e04031. DOI: 10.1016/j.heliyon.2020.e04031.

Arumugam, P., Chemura, A., Aschenbrenner, P. et al. (2023). Climate change impacts and adaptation strategies: An assessment on sorghum for Burkina Faso. *Eur. J. Agron.*, 142, 126655. DOI: 10.1016/j.eja.2022.126655.

Ascott, M., Macdonald, D., Sandwidi, W. et al. (2022). Time of emergence of impacts of climate change on groundwater levels in sub-saharan Africa. *J. Hydrol.*, 612, 128107. DOI: 10.1016/j.jhydrol.2022.128107.

Augusseau, X., Cuisance, D., Michel, J.F. et al. (2001). Modélisation de "paysage épidémiologiquement dangereux" par télédétection et SIG. *L'Information Géographique*, 65, 73–80. DOI: 10.3406/ingeo.2001.2738.

Ayanlade, A., Oluwaranti, A., Ayanlade, O.S. et al. (2022). Extreme climate events in sub-saharan Africa: A call for improving agricultural technology transfer to enhance adaptive capacity. *Clim. Serv., 27*, 100311. DOI: 10.1016/j.cliser.2022.100311.

Azibo, B.R., and Kimengsi, J.N. (2015). Building an Indigenous Agro-pastoral Adaptation Framework to Climate Change in sub-saharan Africa: Experiences from the North West Region of Cameroon. *Procedia Environ. Sci.*, 29, 126–127. DOI: 10.1016/j.proenv.2015.07.214.

Balima, L.H., Kouamé, F.N., Bayen, P. et al. (2021). Influence of climate and forest attributes on aboveground carbon storage in Burkina Faso, West Africa. *Environ. Challen.*, 4, 100123. DOI: 10.1016/j.envc.2021.100123.

Ballouche, A. (1998). Dynamique des paysages végétaux sahélo-soudaniens et pratiques agro-pastorales à l'holocène: exemples au Burkina Faso (Holocene dynamic of Sahelo-sudanian vegetation landscapes and agro-pastoral practices: examples from Burkina Faso). *Bull. Assoc. Geogr. Fr.*, 75, 191–200. DOI: 10.3406/bagf.1998.2035.

Bandre, E. (1993). La dynamique du couvert végétal dans la région de Gboué, province de la Kossi, Burkina Faso. *Pays enclavés*, 7, 27–46.

Barro, A., Taonda, J.B., Manu, A. et al. (2005). Fight poverty by agricultural production optimization in Burkina Faso using GIS. In Proc. 2005 IEEE International Geoscience and Remote Sensing Symposium. IGARSS'05, 8, 5350–5353. DOI: 10.1109/IGARSS.2005.1525946.

Belemtougri, A.P., Ducharne, A., Tazen, F. et al. (2021). Understanding key factors controlling the duration of river flow intermittency: Case of Burkina Faso in West Africa. *J. Hydrol. Reg.*, 37, 100908. DOI: 10.1016/j.ejrh.2021.100908.

Biasutti, M. (2019). Rainfall trends in the African Sahel: Characteristics, processes, and causes. *WIREs Clim. Change*, 10, e591. DOI: 10.1002/wcc.591.

Bocksberger, G., Schnitzler, J., Chatelain, C. et al. (2016). Zizka, G. Climate and the distribution of grasses in West Africa. *J. Veg. Sci.*, 27, 306–317. DOI: 10.1111/jvs.12360.

Brons, J.E., Zaal, F., Ruben, R. et al. (2000). Climate Change, Agricultural Variability and Risk-coping Strategies. A farm and household level analysis in northern Burkina Faso. Technical report, CERES/WUR/RIVM.

Bunclark, L., Gowing, J., Oughton, E. et al. (2018). Understanding farmers' decisions on adaptation to climate change: Exploring adoption of water harvesting technologies in Burkina Faso. *Glob. Environ. Change*, 48, 243–254. DOI: 10.1016/j.gloenvcha.2017.12.004.

Calzadilla, A., Zhu, T., Rehdanz, K. et al. (2013). Ringler, C. Economywide impacts of climate change on agriculture in sub-saharan Africa. *Ecol. Econ.*, 93, 150–165. DOI: 10.1016/j.ecolecon.2013.05.006.

Capozzi, F., Di Palma, A., De Paola, F. et al. (2018). Assessing desertification in sub-saharan peri-urban areas: Case study applications in Burkina Faso and Senegal. *J. Geochem. Explor.*, 190, 281–291. DOI: 10.101 935 6/j.gexplo.2018.03.012.936.

Cecchi, P., Meunier-Nikiema, A., Moiroux, N. et al. (2008). Towards an atlas of lakes and reservoirs in Burkina Faso.

Da, S.S. (2010). Spatial patterns of West-African plant diversity along a climatic gradient from coast to Sahel. PhD thesis. Universitäts-und Landesbibliothek Bonn.

Daniel, C.C., Thomas, G., Heidi, W. et al. (2013). Farming in the West African Sudan Savanna: Insights in the context of climate change. *Afr. J. Agric. Res.*, 8, 4693–4705. DOI: 10.5897/AJAR2013.7153.

De Longueville, F., Hountondji, Y.C., Kindo, I. et al. (2016). Long-term analysis of rainfall and temperature data in Burkina Faso (1950–2013). *Int. J. Climatol.*, 36, 4393–4405. DOI: 10.1002/joc.4640.

Devineau, J.L., Fournier, A., and Nignan, S. (2010). Savanna fire regimes assessment with MODIS fire data: Their relationship to land cover and plant species distribution in western Burkina Faso (West Africa). *J. Arid Environ.*, 74, 1092–1101. DOI: 10.1016/j.jaridenv.20830 10.03.009.

Dimobe, K., Ouédraogo, A., Soma, S. et al. (2015). Identification of driving factors of land degradation and deforestation in the Wildlife Reserve of Bontioli (Burkina Faso, West Africa). *Glob. Ecol. Conserv.*, 4, 559–571. DOI: 10.1016/j.gecco.2015.10.006.

Dimobe, K., Kouakou, J.L.N., Tondoh, J.E. et al. (2018). Predicting the Potential Impact of Climate Change on Carbon Stock in Semi-Arid West African Savannas. *Land*, 7. DOI: 10.3390/land7040124.

Dimobe, K., Ouédraogo, A., Ouédraogo, K. et al. (2020). Climate change reduces the distribution area of the shea tree (Vitellaria paradoxa C.F. Gaertn.) in Burkina Faso. *J. Arid Environ.*, 181, 104237. DOI: 10.1016/j.jaridenv.2020.104237.

Dimobe, K., Gessner, U., Ouédraogo, K. et al. (2022a). Trends and drivers of land use/cover change in W National park in Burkina Faso. *Environ. Dev.*, 44, 100768. DOI: 10.1016/j.envdev.2022.100768.

Dimobe, K., Ouédraogo, K., Annighöfer, P. et al. (2022b). Climate change aggravates anthropogenic threats of the endangered savanna tree Pterocarpus erinaceus (Fabaceae) in Burkina Faso. *J. Nat. Conserv.*, 70, 126299. DOI: 10.1016/j.jnc.2022.126299.

Emediegwu, L.E., Wossink, A., and Hall, A. (2022). The impacts of climate change on agriculture in sub-saharan Africa: A spatial panel data approach. *World Dev.*, 158, 105967. DOI: 10.1016/j.worlddev.2022.105967.

Etongo, D., Djenontin, I.N.S., Kanninen, M. et al. (2015). Land tenure, asset heterogeneity and deforestation in Southern Burkina Faso. *For. Policy Econ.*, 61, 51–58. DOI: 10.1016/j.forpol.2015.08.006.

Forkuor, G., Dimobe, K., Serme, I., et al. (2018). Landsat-8 vs. Sentinel-2: examining the added value of sentinel-2's red-edge bands to land-use and land-cover mapping in Burkina Faso. *GIsci. Remote Sens.*, 55, 331–354. DOI: 10.1080/15481603.2017.1370169.

Gaetani, M., Janicot, S., Vrac, M. et al. (2020). Robust assessment of the time of emergence of precipitation change in West Africa. *Sci. Rep.*, 10, 7670. DOI: 10.1038/s41598-020-63782-2.

Gaisberger, H., Kindt, R., Loo, J. et al. (2017). Spatially explicit multi-threat assessment of food tree species in Burkina Faso: A fine-scale approach. *PLoS One*, 12, e0184457. DOI: 10.1371/948 journal.pone.0184457.

Gbode, I.E., Diro, G.T., Intsiful, J.D. et al. (2022). Current Conditions and Projected Changes in Crop Water Demand, Irrigation Requirement, and Water Availability over West Africa. *Atmosphere*, 13. DOI: 10.3390/atmos13071155.

GEBCO (2020). GEBCO Compilation Group. GEBCO 2020 Grid. DOI: 10.5285/a29c5465-b138-234d-1075e053-6c86abc040b9.

Hannah, L., Midgley, G., Lovejoy, T. et al. (2002). Conservation of biodiversity in a changing climate. *Conservation Biology*, 16, 264–268. DOI: 10.1046/j.1523-1739.2002.00465.x.

Idrissou, M., Diekkrüger, B., Tischbein, B. et al. (2022). Modeling the Impact of Climate and Land Use/Land Cover Change on Water Availability in an Inland Valley Catchment in Burkina Faso. *Hydro.*, 9. DOI: 10.3390/hydrology9010012.

Kadeba, A., Nacoulma, B.M.I., Ouedraogo, A. et al. (2015). Land cover change and plants diversity in the Sahel: A case study from northern Burkina Faso. *Ann. For. Res.*, 58. DOI: 10.15287/afr.2015.350.

Kanmegne Tamga, D., Latifi, H., Ullmann, T. et al. (2023). Estimation of Aboveground Biomass in Agroforestry Systems over Three Climatic Regions in West Africa Using Sentinel-1, Sentinel-2, ALOS, and GEDI Data. *Sensors*, 23. DOI: 10.3390/s23010349.

Kasei, R., Diekkrüger, B., and Leemhuis, C. (2010). Drought frequency in the Volta Basin of West Africa. *Sustain. Sci.*, 5, 89. DOI: 10.1007/s11625-009-0101-5.

Landmann, T., Machwitz, M., Le, Q.B. et al. (2008). A Land Cover Change Synthesis Study for the GLOWA Volta Basin in West Africa using Time Trajectory Satellite Observations and Cellular Automata Models. In Proc. IGARSS 2008 – IEEE Int. Geosci. Remote Sens., 3, 640–643. DOI: 10.1109/IGARSS.2008.4779429.

Lemenkova, P., and Debeir, O. (2022a). Seismotectonics of Shallow-Focus Earthquakes in Venezuela with Links to Gravity Anomalies and Geologic Heterogeneity Mapped by a GMT Scripting Language. *Sustainability*, 14. DOI: 10.3390/su142315966.

Lemenkova, P., and Debeir, O. (2022b). Satellite Altimetry and Gravimetry Data for Mapping Marine Geodetic and Geophysical Setting of the Seychelles and the Somali Sea, Indian Ocean. *J. Appl. Eng. Sci.*, 12, 191–202. DOI: 10.2478/jaes-2022-0026.

Lemenkova, P., and Debeir, O. (2022c). Satellite Image Processing by Python and R Using Landsat 9 OLI/TIRS and SRTM DEM Data on Côte d'Ivoire, West Africa. *J. Imaging*, 8. DOI: 10.3390/jimaging8120317.

Lemenkova, P., and Debeir, O. (2022d). R Libraries for Remote Sensing Data Classification by K-Means Clustering and NDVI Computation in Congo River Basin, DRC. *Appl. Sci.*, 12. DOI: 10.3390/app122412554.

Lemenkova, P., and Debeir, O. (2023). Quantitative Morphometric 3D Terrain Analysis of Japan Using Scripts of GMT and R. *Land*, 12. DOI: 10.3390/land12010261.

Machwitz, M., Landmann, T., Conrad, C. et al. (2008). Land Cover Analysis on Sub-Continental Scale: FAO LCCS Standard with 250 Meter MODIS Satellite Observations in West Africa. In Proceedings of the IGARSS 2008 – 2008 IEEE Int. Geosci. Remote. Sens. Symposium, 5, 49–52. DOI: 10.1109/IGARSS.2008.4780024.

Martino, G.D., Iodice, A., Riccio, D. et al. (2011). Use of High Resolution Satellite Images for the Calibration of Hydro-geological Models in Semi-Arid Regions: A Case Study. In Proc. 2011 IEEE Global Humanitarian Technology Conference, 171–175. DOI: 10.1109/GHTC.2011.80.

Mather, J.R. (1987). *Vegetation and climate*. Climatology, Springer US: Boston, MA. 902–910. DOI: 10.1007/0-387-30749-4_189.

Miura, Y., Eriksson, L.E.B., Ostwald, M. et al. (2019). Soil Moisture Monitoring of Agricultural Fields in Burkina Faso Using Dual Polarized Sentinel-1a Data. In Proc. IGARSS 2019 – 2019 IEEE Int. Geosci. Remote. Sens. Symposium, 7045–7048. DOI: 10.1109/IGARSS.2019.889 8897.

Moser, L., Voigt, S., Schoepfer, E. et al. (2014). Multitemporal Wetland Monitoring in sub-saharan West-Africa Using Medium Resolution Optical Satellite Data. *IEEE J. Sel. Top. Appl. Earth Obs. Remote Sens.*, 7, 3402–3415. DOI: 10.1109/JSTARS.2014.2336875.

Musyimi, Z., Said, M.Y., Zida, D. et al. (2017). Aynekulu, E. Evaluating fire severity in Sudanian ecosystems of Burkina Faso using Landsat 8 satellite images. *J. Arid Environ.*, 139, 95–109. DOI: 10.1016/j.jaridenv.2016.11.005.

Nebie, O. (1993). Les problèmes d'aménagement et de gestion des terroirs villageois dans le Sahel burkinabé – Exemples de Koria, Seytenga, Titabé, Boundoré (Province du Séno). Pays enclavés, 7, 61–83. Included in a thematic issue: Aspects des milieux naturels du Burkina Faso.

Offerle, B., Jonsson, P., Eliasson, I. et al. (2005). Urban modification of the surface energy balance in the West African Sahel: Ouagadougou, Burkina Faso. *J. Clim.*, 18, 3983–3995. DOI: 10.1175/JCLI3520.1.

Ofori-Sarpong, E. (1987). Hargreaves' climatic classification and crop zonation in Burkina Faso*. *J. Arid Environ.*, 12, 179–185. DOI: 10.1016/S0140-1963(18)31189-3.

Oguntunde, P.G., Friesen, J., van de Giesen, N. et al. (2006). Hydroclimatology of the Volta River Basin in West Africa: Trends and variability from 1901 to 2002. *Phys. Chem. Earth, Parts A/B/C*, 31, 1180–1188. DOI: 10.1016/j.pce.2006.02.062.1052.

Okafor, G.C., Larbi, I., Chukwuma, E.C. et al. (2021). Local climate change signals and changes in climate extremes in a typical Sahel catchment: The case of Dano catchment, Burkina Faso. *Environ. Challeng.*, 5, 100285. DOI: 10.1016/j.envc.2021.100285.

Olsson, L. (1993). Desertification in Africa – a critique and an alternative approach. *GeoJournal*, 31, 23–31. DOI: 10.1007/BF00815899.

Op de Hipt, F., Diekkrüger, B., Steup, G. et al. (2018). Modeling the impact of climate change on water resources and soil erosion in a tropical catchment in Burkina Faso, West Africa. *CATENA*, 163, 63–77. DOI: 10.1016/j.catena.2017.11.023.

Op de Hipt, F., Diekkrüger, B., Steup, G. et al. (2019). Modeling the effect of land use and climate change on water resources and soil erosion in a tropical West African catchment (Dano, Burkina Faso) using SHETRAN. *Sci. Total Environ.*, 653, 431–445. DOI: 10.1016/j.scitotenv.2018.10.351.

Ouedraogo, B.I., Tigabu, M., Savadogo, P. et al. (2010). Land cover change and its relation with population dynamics in Burkina Faso, West Africa. *Land Degrad. Dev.*, 21, 453–462. DOI: 10.1002/ldr.981.

Ouedraogo, B.I., Levermore, G.J., and Parkinson, J.B. (2012). Future energy demand for public buildings in the context of climate change for Burkina Faso. *Build. Environ.*, 49, 270–282. DOI: 10.1016/j.buildenv.2011.10.003.

Ouédraogo, R.A., Kambiré, F. C., Kestemont, M.-P. et al. (2019). Caractériser la diversité des exploitations maraîchères de la région de Bobo-Dioulasso au Burkina Faso pour faciliter leur transition agroécologique. *Cah. Agric.*, 28, 20. DOI: 10.1051/cagri/2019021.

R Core Team (2022). R: A Language and Environment for Statistical Computing. R Foundation for Statistical Computing, Vienna, Austria. URL: https://www.R-project.org/.

Rasmussen, K., Fog, B., and Madsen, J.E. (2001). Desertification in reverse? Observations from northern Burkina Faso. *Glob. Environ. Change*, 11, 271–282. DOI: 10.1016/S0959- 3780(01)00005-X.

Reij, C., Tappan, G., and Belemvire, A. (2005). Changing land management practices and vegetation on the Central Plateau of Burkina Faso (1968–2002). *J. Arid Environ.*, 63, 642–659. DOI: 10.1016/j.jaridenv.2005.03.010.

Richards, J.A. (2013). *Remote Sensing Digital Image Analysis. An Introduction*. Springer: Dordrecht, 834 Netherlands. DOI: 10.1007/978-3-642-30062-2.

Rigolot, C., de Voil, P., Douxchamps, S. et al. (2017). Interactions between intervention packages, climatic risk, climate change and food security in mixed crop–livestock systems in Burkina Faso. *Agric. Syst.*, 151, 217–224. DOI: 10.1016/j.agsy.2015.12.017.

Rochette, R.M. (1989). Le Sahel en lutte contre la désertification: leçons d'expériences.

Salter, P.J., and Goode, J.E. (1967). Crop responses to water at different stages of growth responses to water at different stages of growth.

Sanou, D.C. (1993). Ruissellement et érosion sur petits bassins versants: le cas de Imiga/Tibin. Pays enclavés, 7, 85–114.

Sawadogo, B. (2022). Drought Impacts on the Crop Sector and Adaptation Options in Burkina Faso: Agender-Focused Computable General Equilibrium Analysis. *Sustainability*, 14. DOI: 10.3390/su142315637.

Séogo, W., and Zahonogo, P. (2023). Do land property rights matter for stimulating agricultural productivity? Empirical evidence from Burkina Faso. Land Use Policy, 125, 106475. DOI: 10.1016/j.landusepol.2022.106475.

Sorgho, R., Jungmann, M., Souares, A. et al. (2021). Climate Change, Health Risks, and Vulnerabilities in Burkina Faso: A Qualitative Study on the Perceptions of National Policymakers. *Int. J. Environ. Res. Public Health*, 18. DOI: 10.3390/ijerph18094972.

Soumaré, M., Havard, M., and Bachelier, B. (2021). Cotton in West and Central Africa: from the agricultural revolution to the agro-ecological transition. *Cah. Agric.*, 30, 5. DOI: 10.1051/cagri/2020044.

Tarchiani, V., Coulibaly, H., Baki, G. et al. (2021). Access, Uptake, Use and Impacts of Agrometeorological Services in Sahelian Rural Areas: The Case of Burkina Faso. *Agronomy*, 11. DOI: 10.3390/agronomy11122431.

USGS (2015). Landsat – Earth observation satellites. Technical report, USGS, U.S.. DOI: 10.3133/fs20153081.

USGS (2022). Landsat 9 Data Users Handbook. online. 1079 EROS Sioux Falls, South Dakota, U.S. LSDS-2082 Version 1.0.

Vall, E., Marre-Cast, L., and Kamgang, H. J. (2017). Chemins d'intensification et durabilité des exploitations de polyculture-élevage en Afrique subsaharienne: contribution de l'association agriculture-élevage. *Cah. Agric.*, 26, 25006. DOI: 10.1051/cagri/201701-990-1.

Vanhuysse, S., Grippa, T., Lennert, M. et al. (2017). Contribution of nDSM derived from VHR stereo imagery to urban land-cover mapping in sub-saharan Africa. In Proc. 2017 Joint Urban Remote Sensing Event (JURSE), 1–4. DOI: 10.1109/ JURSE.2017.7924570.

Van Teeffelen, P., de Jong, S., and van den Berg, L. (2001). Urban monitoring: new possibilities of combining high spatial resolution IKONOS images with contextual image analysis techniques. In Proc. IEEE/ISPRS Joint Workshop on Remote Sensing and Data Fusion over Urban Areas (Cat. No.01EX482), 265–269. DOI: 10.1109/DFUA.2001.985893.

Wagner, W., and Scipal, K. (2000). Large-scale soil moisture mapping in western Africa using the ERS scatterometer. *IEEE Trans. Geosci. Remote Sens.*, 38, 1777–1782. DOI: 10.1109/36.851761.

Waha, K., Müller, C., Bondeau, A. et al. (2013). Adaptation to climate change through the choice of cropping system and sowing date in sub-saharan Africa. *Glob. Environ. Change*, 23, 130–143. DOI: 10.1016/j.918 gloenvcha.2012.11.001.

Waongo, M., Laux, P., and Kunstmann, H. (2015). Adaptation to climate change: The impacts of optimized planting dates on attainable maize yields under rainfed conditions in Burkina Faso. *Agric. For. Meteorol.*, 205, 23–39. DOI: 10.1016/j.agrformet.2015.02.006.

Webber, H., Gaiser, T., and Ewert, F. (2014). What role can crop models play in supporting climate change adaptation decisions to enhance food security in sub-saharan Africa? *Agric. Syst.*, 127, 161–177. DOI: 10.1016/j.agsy.2013.12.006.

Wessel, P., and Smith, W.H.F. (1991). Free software helps map and display data. *Eos Trans. AGU*, 72(41), 441–446. DOI: 10.1029/90EO00319.

Wessel, P., Luis, J.F., Uieda, L. et al. (2019). The Generic Mapping Tools version 6. *Geochem. Geophys. Geosys.*, 20, 5556–5564. DOI: 10.1029/2019GC008515.

Wilmet, J. (1986). Analyse géographique et télédétection spatiale à haute résolution. *Bulletins de l'Académie Royale de Belgique*, 72, 381–392. DOI: 10.3406/barb.1986.61410.

Zoungrana, B.J.B., Conrad, C., Amekudzi, L.K. et al. (2015). Multi-Temporal Landsat Images and Ancillary Data for Land Use/Cover Change (LULCC) Detection in the Southwest of Burkina Faso, West Africa. *Remote Sens.*, 7, 12076–12102. DOI: 10.3390/rs70912076.

Zoungrana, B.J.B., Conrad, C., Thiel, M. et al. (2018). MODIS NDVI trends and fractional land cover change for improved assessments of vegetation degradation in Burkina Faso, West Africa. *J. Arid Environ.*, 153, 66–75. DOI: 10.1016/j. Jaridenv.2018.01.005.

Zougmoré, R.B., Partey, S.T., Ouédraogo, M. et al. (2018). Facing climate variability in sub-saharan Africa: analysis of climate-smart agriculture opportunities to manage climate-related risks. *Cah. Agric.*, 27, 34001. DOI: 10.1051/cagri/2018019.